# On the Discretization Error of the Discrete Generalized Quantum Master Equation

Ruojing Peng,<sup>1</sup> Lachlan P. Lindoy,<sup>2</sup> and Joonho Lee<sup>1,\*</sup>

<sup>1</sup>Department of Chemistry and Chemical Biology,
Harvard University, Cambridge, MA 02138, USA

<sup>2</sup>National Physical Laboratory, Teddington, TW11 0LW, United Kingdom

The transfer tensor method (TTM) [Cerrillo and Cao, Phys. Rev. Lett. 2014, 112, 110401] can be considered a discrete-time formulation of the Nakajima-Zwanzig quantum master equation (NZ-QME) for modeling non-Markovian quantum dynamics. A recent paper [Makri, J. Chem. Theory Comput. 2025, 21, 5037] raised concerns regarding the consistency of the TTM discretization, particularly a spurious term at the initial time t=0. This Communication presents a detailed analysis of the discretization structure of TTM, clarifying the origin of the initial-time correction and establishing a consistent relationship between the TTM discrete-time memory kernel  $K_N$ , and the continuous-time NZ-QME kernel  $\mathcal{K}(N\Delta t)$ . This relationship is validated numerically using the spin-boson model, demonstrating convergence of reconstructed memory kernels and accurate dynamical evolution as  $\Delta t \to 0$ . While TTM provides a consistent discretization, we note that alternative schemes are also viable, such as the midpoint derivative/midpoint integral scheme proposed in Makri's work. The relative performance of various schemes for either computing accurate  $\mathcal{K}(N\Delta t)$  from exact dynamics, or obtaining accurate dynamics from exact  $\mathcal{K}(N\Delta t)$ , warrants further investigation.

### I. INTRODUCTION

The Nakajima-Zwanzig quantum master equation (NZ-QME) [1, 2] offers a formally exact approach for simulating non-Markovian open quantum dynamics, focusing only on quantities of the dimension of the systems. Of central importance in the NZ-QME formulism is the time-non-local memory kernel K(t), which accounts for the non-Markovian effect of environment, and is related to influence functional [3] of the path integral approach [4–12]. The NZ-QME memory kernel  $\mathcal{K}(t)$  can be computed from various approximate schemes, such as Bloch-Redfield equations [13, 14], coupled integral equation [15–17], or from reduced dynamical channels on a dense time grid [18-20]. A closely related alternative is the transfer tensor method (TTM) [21] by Cerrillo and Cao, which computes discrete time memory kernels  $K_n$ from dynamical channels on a coarse time grid. Being a highly efficient data-driven approach, TTM has demonstrated its efficiency and accuracy for a variety of systems [22–25], and combines easily with quantum tomography [26, 27].

In the original Refs. 21 and 26, the TTM discrete time memory kernel  $K_n$  was simply related to the NZ-GME continuous time memory kernel  $\mathcal{K}(n\Delta t)$  at each discrete time point (see, e.g., Eq. (5) in Ref. 21 and Eq. (12) in Ref. 26). In addition, Ref. 21 numerically demonstrated that  $K_n$  computed from TTM equation converges to  $\mathcal{K}(n\Delta t)$  in the  $\Delta t \to 0$  limit for time points n > 0 (Fig.4 in Ref. 21). A recent paper [28] by Makri raised a concern on the relationship between  $K_n$  and  $\mathcal{K}(n\Delta t)$ . In particular,  $K_0$  is identified as a spurious term, which leads to wrong dynamics, while the simple identification

In this Communication, we present an analysis to clarify the apparent inconsistency in the discretized GQME. Section II provides a detailed analysis of the relation between  $K_n$  from the TTM equations and  $\mathcal{K}(n\Delta t)$  in the NZ-QME, with a consistent treatment of initial time, much of which was contained in the addendum to our recent work [3]. Section III provides numerical evidence for the relationship derived in Section II.

### II. DISCRETIZATION ERROR ANALYSIS

A detailed analysis of discretization error in the TTM equation is provided in Ref. 3 (Addendum). Here, we provide a sketch of the analysis for completeness, emphasizing the subtleties associated with the initial time.

The continuous-time homogeneous NZ equation [1, 2, 15] for the system propagator U(t) is

$$\dot{U}(t) = -iL_s U(t) + \int_0^t d\tau \mathcal{K}(\tau) U(t - \tau) \tag{1}$$

where  $L_s = [H_s, \cdot]$  and U(t) is defined by  $\rho(t) = U(t)\rho(0)$ . For the subsequent analysis, it is useful to write its second-order derivative, as derived in Ref. 19,

$$\ddot{U}(t) = (-iL_s)^2 U(t) + \mathcal{K}(t) + \int_0^t d\tau \mathcal{F}(\tau) U(t-\tau), \quad (2)$$

where

$$\mathcal{F}(t) = \{\mathcal{K}(t), -iL_s\} + \int_0^t d\tau \mathcal{K}(\tau) \mathcal{K}(t-\tau), \qquad (3)$$

of  $K_n$  with  $\mathcal{K}(n\Delta t)$  remains numerically valid for n > 0. Furthermore, Ref. 28 proposed an alternative discretization scheme for NZ-QME using exact  $\mathcal{K}(n\Delta t)$ .

<sup>\*</sup> joonholee@g.harvard.edu

and the third-order derivative

$$\ddot{U}(t) = \left[ (-iL_s)^3 + \{\mathcal{K}_0, -iL_s\} + \dot{\mathcal{K}}_0 \right] U(t) 
+ \int_0^t d\tau \mathcal{R}(t-\tau) U(\tau),$$
(4)

where

$$\mathcal{R}(t) = \left[ \left[ (-iL_s)^2 + \mathcal{K}_0 \right] \mathcal{K} - iL_s \dot{\mathcal{K}} + \ddot{\mathcal{K}} \right] (t).$$
 (5)

We note that  $\mathcal{F}(t) \sim \mathcal{O}(||\mathcal{K}(t)||)$  ( $||\cdot||$  denotes Frobenius norm of the matrix) from Young's convolution inequality [29, 30]. Furthermore,  $\dot{\mathcal{K}}(t)$ ,  $\ddot{\mathcal{K}}(t)$ , and hence  $\mathcal{R}(t)$  are also  $\mathcal{O}(||\mathcal{K}(t)||)$  from the projection of full system-and-bath evolution [16, 17].

We now consider the discrete-time version of Eqs. (1), (2) and (4). Following the same convention as our original manuscript (Ref. [3]), let  $t = N\Delta t$ ,  $L = I - i\Delta t L_s$ ,  $\rho_N = \rho(N\Delta t)$ ,  $U_N = U(N\Delta t)$ . Furthermore, we denote by  $\mathcal{K}_m = \mathcal{K}(m\Delta t)$  the continuous-time memory kernel in Eq. (1) evaluated at discrete time steps, and denote by  $K_m$  the discrete-time memory kernel defined by discrete time relations

$$U_{N+1} = LU_N + \Delta t^2 \sum_{m=0}^{N} K_m U_{N-m}, \tag{6}$$

from Ref. [3]. At this point, we also note that  $\mathcal{K}_m$  may not be straightforwardly related to  $K_m$  and could not be the same as  $K_m$  in the limit of  $\Delta t \to 0$ . One must conduct a careful discretization analysis to examine this relationship and equivalence, which is the primary purpose of this Communication. In the following analysis, we assume that  $\{U_m\}$  are exact, which recovers the TTM [21]. We demonstrate how the discretization error in the discrete NZ equation propagates into the relationship between  $\mathcal{K}_m$  and  $K_m$ .

We begin by considering the time derivatives of the system propagator at t = 0 (i.e., N = 0),

$$\ddot{U}_0 = (-iL_s)^2 + \mathcal{K}_0,\tag{7}$$

$$\ddot{U}_0 = (-iL_s)^3 + \{\mathcal{K}_0, -iL_s\} + \dot{\mathcal{K}}_0. \tag{8}$$

The expansion of  $U_1$  at t=0 follows,

$$U_1 = I + \Delta t \dot{U_0} + \frac{\Delta t^2}{2} \ddot{U_0} + \frac{\Delta t^3}{6} \ddot{U_0} + \mathcal{O}(\Delta t^4).$$
 (9)

We can use Eqs. (6) and (9) to obtain

$$K_0 = \frac{1}{2} \left( (-iL_s)^2 + \mathcal{K}_0 \right) + \frac{\Delta t}{6} \ddot{U}_0 + \mathcal{O}(\Delta t^2).$$
 (10)

Note that Eq. (10) is different from the simple assignment  $K_0 = \mathcal{K}_0$  in Ref. 21 (see Eq. (5) therein, and Eq. (12) in Ref. 26). Here, the continuous time  $\mathcal{K}_0$  is a well-defined *non-trivial* quantity, whose expression in terms of projectors is [16, 17]

$$\mathcal{K}_0 = -\text{Tr}_{\text{bath}}[L(I-P)L\rho_{\text{bath}}],$$
 (11)

where  $L = [H, \cdot]$  is the Liouvillian of the full system and bath space, and  $P(\cdot) = \rho_{\text{bath}} \otimes \text{Tr}_{\text{bath}}(\cdot)$  is the projector onto the system. In particular, the effect of  $\mathcal{K}_0$  enters even in the propagation from  $U_0$  to  $U_1$ , unlike hypothesized in Ref. 28 (see, e.g., Eq. (12) and Eq. (18) therein). As worked out in the following, the "convolution integral overestimation" pointed out in Ref. 28 can be considered as a way to correctly account for the  $\mathcal{O}(\Delta t^2 \ddot{U}_N)$  term in time-propagation from  $U_N$  to  $U_{N+1}$ .

For N > 0, we discretize the time-convolution integral in Eqs. (2) and (4) with the right Riemann sum,

$$\ddot{U}_N = (-iL_s)^2 U_N + \mathcal{K}_N + \Delta t \sum_{m=1}^N \mathcal{F}_m U_{N-m} 
+ \Delta t^2 \sum_{m=1}^N D_m^{\mathcal{F}},$$
(12)

$$\ddot{U}_{N} = \ddot{U}_{0}U_{N} + \Delta t \sum_{m=1}^{N} \mathcal{R}_{m}U_{N-m} + \Delta t^{2} \sum_{m=1}^{N} D_{m}^{\mathcal{R}}, (13)$$

where

$$D_m^X \sim \frac{d}{d\tau} \left[ X(\tau) U(N\Delta t - \tau) \right]_{\tau = m\Delta t}$$
 (14)

for  $X = \mathcal{F}, \mathcal{R}$ . Next, the integral in Eq. (1) is approximated by the trapezoidal rule,

$$\dot{U}_{N} = -iL_{s}U_{N} + \Delta t \left[ \frac{1}{2} \mathcal{K}_{N} + \sum_{m=1}^{N-1} \mathcal{K}_{m}U_{N-m} + \frac{1}{2} \mathcal{K}_{0}U_{N} \right] + \Delta t^{3} \sum_{m=1}^{N} D_{m}^{\mathcal{K}},$$
(15)

where

$$D_m^{\mathcal{K}} \sim \frac{d^2}{d\tau^2} \left[ \mathcal{K}(\tau) U(t - \tau) \right]_{\tau = m\Delta t}. \tag{16}$$

Similarly to Eq. (9), the expansion of  $U_{N+1}$  at  $t = N\Delta t$  follows

$$U_{N+1} = U_N + \Delta t \dot{U}_N + \frac{\Delta t^2}{2} \ddot{U}_N + \frac{\Delta t^3}{6} \ddot{U}_N + \mathcal{O}(\Delta t^4)$$

$$= LU_N + \Delta t^2 \left[ \sum_{m=1}^N \mathcal{K}_m U_{N-m} + K_0 U_N \right]$$

$$+ \frac{\Delta t^3}{2} \sum_{m=1}^N \mathcal{F}_m U_{N-m} + \mathcal{O}\left(\Delta t^4 \sum_{m=1}^N (D_m^{\mathcal{K}} + D_m^{\mathcal{F}})\right)$$

$$+ \frac{\Delta t^4}{6} \sum_{m=0}^{N-1} \mathcal{R}_{N-m} U_m + \mathcal{O}\left(\Delta t^5 \sum_{m=1}^N D_m^{\mathcal{R}}\right). \quad (17)$$

Finally, by comparing Eq. (6) and Eq. (17), we observe

$$K_N = \mathcal{K}_N + \frac{\Delta t}{2} \mathcal{F}_N + \mathcal{O}\left(\Delta t^2 (D_N^{\mathcal{K}} + D_N^{\mathcal{F}})\right). \tag{18}$$

Eqs. (10) and (18) shows the relationship between  $K_N$  and  $\mathcal{K}_N$  as follows: Up to  $O(\Delta t)$ ,  $K_N$  agrees with  $\mathcal{K}_N$  for N>0, and  $K_0=(-L_s^2+\mathcal{K}_0)/2$ ; this way of relating  $\mathcal{K}_N$  and  $K_N$  will henceforth be called TTM(1). Furthermore, given exact  $U_0$  and  $\mathcal{F}_n$ ,  $\mathcal{K}_N$  and  $K_N$  can be computed from each other with  $O(\Delta t^2)$  error for all  $N\geq 0$  using Eqs. (10) and (18); we refer to this scheme as TTM(2). Note that the TTM(2) scheme requires accurate computation of  $U_0$  and  $\mathcal{F}_n$ . In particular, the integral in Eq. (3) needs to be computed on dense grid, making the TTM(2) scheme much more costly. In any case, our analysis reveals that the simple identification of  $K_N$  with  $\mathcal{K}_N$  (e.g. Eq. (5) in Ref. 21 and Eq. (12) in Ref. 26) are valid for N>0, and needs to be corrected as Eq. (10) for N=0.

We stress that Eqs. (10) and (18) only applies when one computes  $\mathcal{K}_N$  from exact  $U_N$  at discrete times. From this perspective, the TTM(1) and TTM(2) schemes can be considered as alternative ways to extract continuous time memory kernels  $\{\mathcal{K}_m\}$  (at discrete time points) from dynamics simulation, with controllable error. In particular,  $\{U_m\}$  and  $\{\mathcal{K}_m\}$  are only computed on coarse time grid in the TTM(1) scheme, whereas existing approaches typically involves integral equations hence requires  $\{U_m\}$  and  $\{\mathcal{K}_n\}$  with fine time resolution [15, 16, 19, 31–35].

Another use case is propagating  $U_N$  according to Eq. (6), using  $K_N$  computed from exact  $\mathcal{K}_N$  as in Eqs. (10) and (18). In this case, the above analysis does not quantify how the discretization error propagates. In the next section, we will present numerical results for the various schemes in both scenarios: computing  $\mathcal{K}_N$  from the exact  $U_N$ , and computing  $U_N$  from the exact  $\mathcal{K}_N$ .

In Ref. 28, an alternative discretization scheme was proposed using the midpoint derivative and midpoint integrals to improve accuracy. In this scheme (hereafter denoted as MPD/I), the discrete time memory kernels  $T_N$  are computed as

$$\frac{1}{2}T_1 = U_1 - \frac{1}{2}G_1 \tag{19}$$

$$\frac{1}{2}T_N = U_N - \sum_{m=1}^{N-1} T_{N-m} U_m, \quad N > 1,$$
 (20)

and  $\mathcal{K}_N$  computed from  $T_N$  as

$$\Delta t^2 G_{1/2} \mathcal{K}_{1/2} = T_1 - G_1 \tag{21}$$

$$\Delta t^2 G_{1/2} \mathcal{K}_{N-1/2} = T_N, \quad N > 1$$
 (22)

where  $G_1 = e^{-i\Delta t L_s}$  and  $G_{1/2} = e^{-i\Delta t L_s/2}$ , and  $\mathcal{K}_N = (\mathcal{K}_{N-1/2} + \mathcal{K}_{N+1/2})/2$  [36]. We will also compare the TTM(1) and TTM(2) schemes with MPD/I in the numerical results.

Finally, we emphasize that the original TTM method [21] uses only discrete time memory kernel  $\{K_m\}$  to propagate dynamics, which in turn are computed from short time dynamical channels  $\{U_m\}$ , both according to Eq. (6). In particular, it does not require a continuous-time memory kernel  $\{\mathcal{K}_n\}$  and is free of any additional discretization error beyond that of  $\{U_m\}$ . Hence, given

exact short time  $\{U_m\}$ , the only error in the original TTM method comes from memory time truncation, i.e., assuming  $K_n = 0$  for all  $n > n_T$  in Eq. (6), where  $n_T$  is some memory truncation time.

### III. NUMERICAL RESULTS AND DISCUSSION

We now move to numerical illustrations of our analysis. We will consider the archetypal open-quantum system Hamiltonian, the spin-boson model Hamiltonian, given as

$$\hat{H} = \hat{H}_s + \hat{H}_b \tag{23}$$

$$\hat{H}_s = \epsilon \sigma_z + \Omega \sigma_x \tag{24}$$

$$\hat{H}_b = \sum_j \frac{\hat{p}_j^2}{2m} + \frac{1}{m} \omega_j^2 \hat{q}_j^2 - c_j \hat{q}_j \sigma_z,$$
 (25)

where  $\sigma_z$ ,  $\sigma_x$  are Pauli matrices,  $\omega_j$  and  $c_j$  are bath frequencies and system-bath coupling coefficients collectively specified through the spectral density function

$$J(\omega) = \frac{\pi}{2} \xi \left( \frac{\omega^s}{\omega_c^{s-1}} \right) e^{-\omega/\omega_c}, \tag{26}$$

where  $\omega_c$  is the cutoff frequency and  $\xi$  is the Kondo parameter. For comparison, we use the same parameters as in Ref. 28:  $\epsilon = 0$ ,  $\Omega = -1$ , s = 1,  $\omega_c = 5$ ,  $\xi = 0.3$  and inverse temperature  $\beta = 5$ .

Furthermore, in the following, the exact  $U_N$  are assembled from simulation of independent trajectories using the hierarchical equation of motion (HEOM) [37–41] combined with a tensor network representation of the Auxiliary Density Operators (ADOs) [42–44] (further details of the implementation are provided in Ref. 3). In each of these calculations, the bath correlation function was fit to a sum-of-exponential form

$$C(t) = \sum_{k=1}^{K} \alpha_k e^{-\nu_k t},$$
 (27)

using the Adaptive Antoulas-Anderson (AAA) algorithm [45] to construct a rational function approximation to the bath spectral function [39]. For the ohmic spin-boson model considered here, a total of K=7 terms were sufficient to accurately capture the bath correlation function over the time scales considered, corresponding to a hierarchy of ADOs containing 14 modes. A direct product basis was used for the hierarchy of ADOs, with each mode, k, truncated at a depth

$$L_k = \min\left(L_{\max}, \max\left(L_{\min}, \frac{L_{\max}\nu_{\min}}{\operatorname{Re}(\nu_k)}\right)\right),$$
 (28)

where  $L_{\rm max}=20$  is the maximum allowed depth for a given mode,  $L_{\rm min}=8$  is the minimum depth to use for any given mode, and  $\nu_{\rm min}$  is the smallest decay rate in

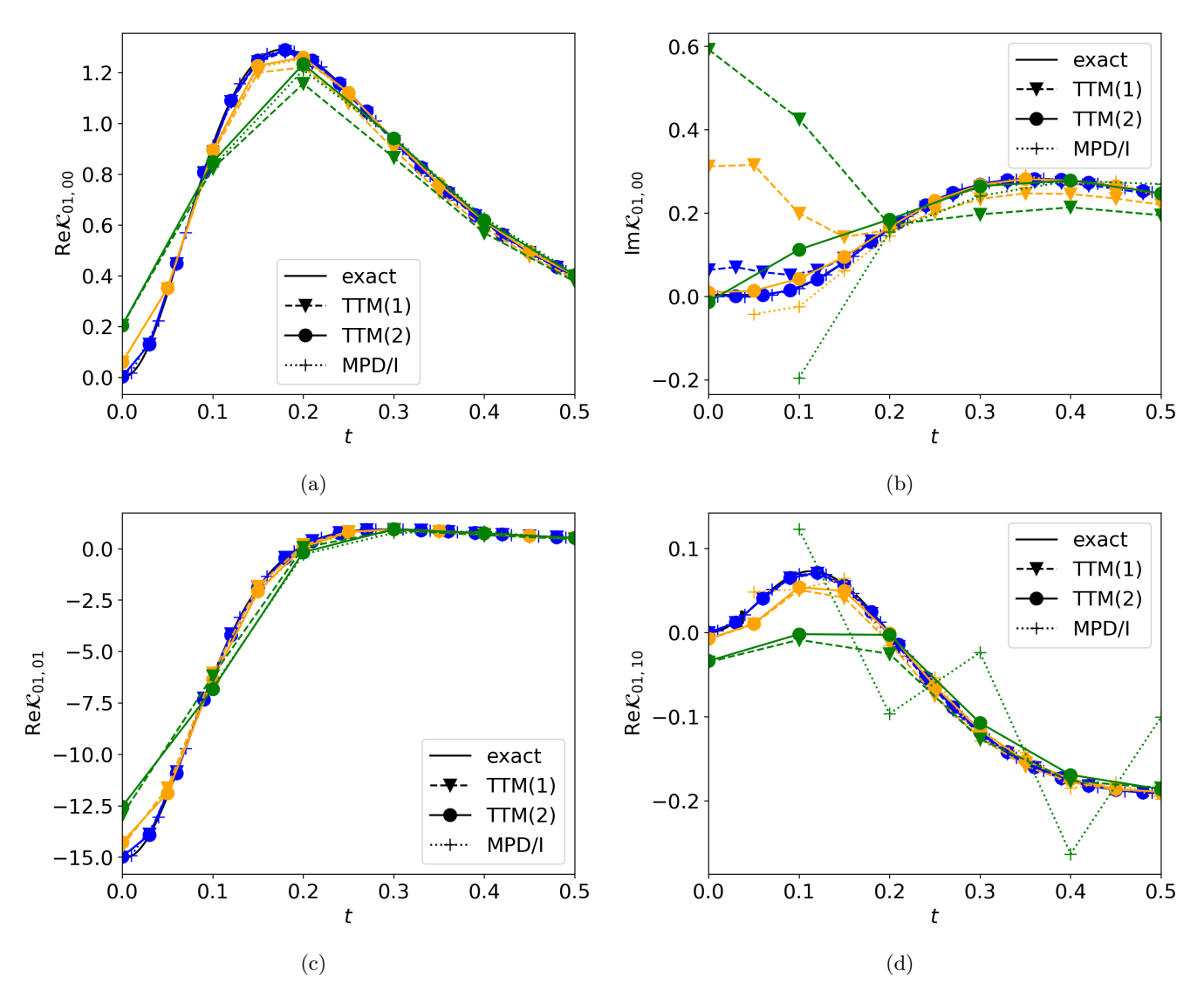


FIG. 1: Elements of continuous time memory kernel  $\mathcal{K}$  from TTM(1), TTM(2) and MPD/I, with corresponding markers labeled as in the plot. Exact results are shown in the black solid curve without a marker. Blue, orange, and green correspond to  $\Delta t = 0.01$ , 0.05, and 0.1, respectively.

the sum-of-exponential decomposition of the bath correlation function. Then  $\mathcal{K}_N$  are the numerically converged solutions of the integro-differential equation as described in Ref. 19, and  $\mathcal{F}_N$  are computed from Eq. (3). To compute the numerically "exact"  $\mathcal{K}_N$ ,  $\mathcal{F}_N$ , and  $U_0$ , we use a small time step size,  $\Delta t_{\rm ref} = 0.0005$ , unless specified otherwise.

We first consider computing  $\mathcal{K}_N$  from exact  $U_N$ . Fig. 1 plots the elements of  $\mathcal{K}$  (chosen to be the same as in Fig. 3 and Fig. 4 of Ref. 28) computed from discrete memory kernels using various schemes (labeled by different markers and line styles) discussed above. Exact  $\mathcal{K}$  are shown in black solid curves without markers. We first note that at N=0,  $\mathcal{K}_0$  computed from both TTM schemes converges to the exact result as  $\Delta t \to 0$ , suggesting that the "spurious term" identified in Ref. 28 can indeed be cor-

rected by Eq. (10). Furthermore, MPD/I is not uniformly more accurate than TTM(1) with the same  $\Delta t$ : For real and imaginary part of  $\mathcal{K}_{01,00}$  (Fig. 1a and Fig. 1b), we reproduce the results in Fig. 4 of Ref. 28, where MPD/I is indeed more accurate. Yet for Re $\mathcal{K}_{01,01}$  and Re $\mathcal{K}_{01,01}$  (Fig. 1c and Fig. 1d), TTM(1) is as accurate as, if not more accurate than, MPD/I.

Fig. 2a plots the Frobenius norm of error  $||\Delta \mathcal{K}||$  of the various schemes, with the reference  $\mathcal{K}$  computed with  $\Delta t_{\rm ref} = 0.0005$ . We first note that, the MPD/I error  $||\Delta \mathcal{K}_N||$  approaches an N-independent constant in the large N limit, where the constant scales as  $\mathcal{O}(\Delta t^2)$ . In particular, for large N, the MPD/I scheme leads to an error  $\Delta \mathcal{K}_N$  which exceeds the value of  $\mathcal{K}_N$  itself, and hence cannot predict  $\mathcal{K}_N$  correctly. For TTM(1), Eq. (18) predicts an error  $||\Delta \mathcal{K}_N|| = \mathcal{O}(||\mathcal{F}_N||\Delta t)$ , which is numeri-

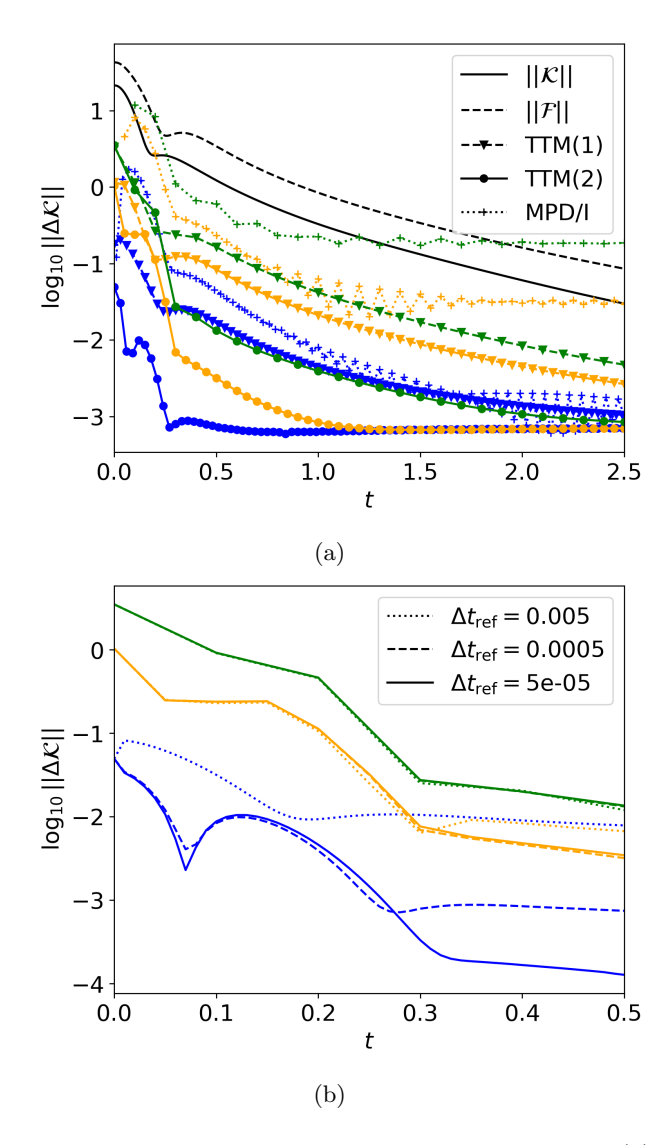


FIG. 2: Error of continuous time memory kernel  $\mathcal{K}$ . (a) Results from TTM(2), TTM(1), and MPD/I schemes are labeled as Fig. 1. Reference  $\log_{10} ||\mathcal{K}_N||$  and  $\log_{10} ||\mathcal{F}_N||$  computed with  $\Delta t_{\rm ref} = 0.0005$  are also plotted in black solid and dashed curves, respectively. (b) TTM(2) results, where the reference  $\mathcal{K}_N$  and  $\mathcal{F}_N$  are computed using increasing  $\Delta t_{\rm ref}$  as labeled. In both panels, blue, orange, and green again correspond to  $\Delta t = 0.01$ , 0.05, and 0.1, respectively.

cally confirmed in Fig. 2a by the decay of  $||\Delta \mathcal{K}||$  which parallels that of  $||\mathcal{F}_{\mathcal{N}}||$ . For TTM(2), Eq. (18) predicts an error  $||\Delta \mathcal{K}_N|| = O\left(\Delta t^2(||D_N^{\mathcal{K}}|| + ||D_N^{\mathcal{F}}||)\right)$ , where  $D_N^{\mathcal{K}}$  and  $D_N^{\mathcal{F}}$  decays as derivatives of  $\mathcal{K}$  and  $\mathcal{F}$ . This is numerically demonstrated in Fig. 2a by the initial fast decay until  $||\Delta \mathcal{K}|| \approx 0.001$ . Furthermore, the saturation at  $||\Delta \mathcal{K}|| \approx 0.001$  is due to numerical error in computing reference  $\mathcal{K}$  and  $\mathcal{F}$  with  $\Delta t_{\rm ref} = 0.0005$ . This is confirmed in Fig. 2b, where the reference  $\mathcal{K}$  and  $\mathcal{F}$  are computed with three different values of  $\Delta t_{\rm ref}$ . In each case, the TTM(2)  $||\Delta \mathcal{K}_N||$  (using different  $\Delta t$ ) decrease with N,

until saturates at around  $2 \times \Delta t_{\rm ref}$ .

Next, we consider simulating dynamics using the exact  $\mathcal{K}_N$ . Fig. 3 plots the long-time system density matrix (RDM) elements  $\text{Re}\rho_{00}$  (solid) and  $\text{Re}\rho_{01}$  (dotted), with initial state  $\rho(0) = |0\rangle\langle 0|$ , and with panel 3a, 3b and 3c corresponds to  $\Delta t = 0.2, 0.1, \text{ and } 0.01$  respectively. In each panel, black curves are the exact results computed from HEOM with time step size  $\Delta t = 0.0005$ . Different discretization schemes are plotted in corresponding colors, where the same memory cutoff  $t_{\text{mem}} = 1.2$  is used as suggested in Ref. 28. In addition, we also plot the result corresponding to simple identification  $K_N = \mathcal{K}_N$ for all  $N \geq 0$  [21, 26], also called "forward-difference approximation with integral overestimation" (FDIO) in Ref. 28. The FDIO results we obtained is manifestly different from that of Ref. 28 (see Fig. 5 therein): (i) our FDIO results shows discretization error as soon as time step N=1, whereas those of Ref. 28 seems numerically exact for  $t < t_{\text{mem}}$ ; (ii) FDIO dynamics in Ref. 28 shows a kink at  $t_{\text{mem}}$ , where as our FDIO dynamics are smooth. However, our FDIO result agrees with that of Ref. 28 in the long time time limit.

Fig. 4 plots the  $\log_{10} || \rho - \rho_{\text{HEOM}} ||$  for the schemes used in Fig. 3 with different  $\Delta t$ , where panel (a),(b),(c) corresponds to TTM(1), TTM(2) and MPD/I, respectively. For each approximation, solid curves correspond to memory cutoff  $t_{\text{mem}} = 1.2$  and dotted curves correspond to  $t_{\text{mem}} = 2.4$ .

Combining observations from Fig. 3 and Fig. 4, we make the following observations: (i) Below the memory cutoff time (i.e.,  $t \leq t_{\text{mem}}$ ), the error convergence in  $O(\Delta t)$  is slowest for TTM(1), and comparable between TTM(2) and MPDI. (ii) Beyond the memory cutoff time, the errors in TTM(1), TTM(2), and MPD/I are all dominated by memory truncation and less affected by discretization error. These observations suggest that, if one can obtain an accurate continuous time memory kernel  $\mathcal{K}_N$  without access to dynamical channels  $U_N$ , then MPD/I could yield accurate short time dynamics than TTM(1) and TTM(2).

## IV. CONCLUSION

This Communication discusses the transfer tensor method (TTM) as a particular discretization of the Nakajima-Zwanzig quantum master equation (NZ-QME). We demonstrated the relationship between the discrete-time memory kernel  $K_N$  in TTM and the continuous-time NZ-QME kernel  $\mathcal{K}(N\Delta t)$ , evaluated at discrete time points, up to an additive  $\mathcal{O}(\Delta t^2)$  error. Specifically, we showed that, for N=0,  $K_0=(-L_s^2+K_0)/2+\Delta t\ddot{U}_0/6+\mathcal{O}(\Delta t^2)$  and for N>0,  $K_N=K_N+\Delta t\mathcal{F}_N/2+\mathcal{O}(\Delta t^2)$ , where  $\mathcal{F}_N$  can be exactly computed from continuous  $\mathcal{K}(t)$ . The truncation at  $\mathcal{O}(\Delta t)$  versus  $\mathcal{O}(\Delta t^2)$  leads to schemes TTM(1) and TTM(2), respectively. In both cases, N=0 can be consistently treated to yield the same time-step error as the other

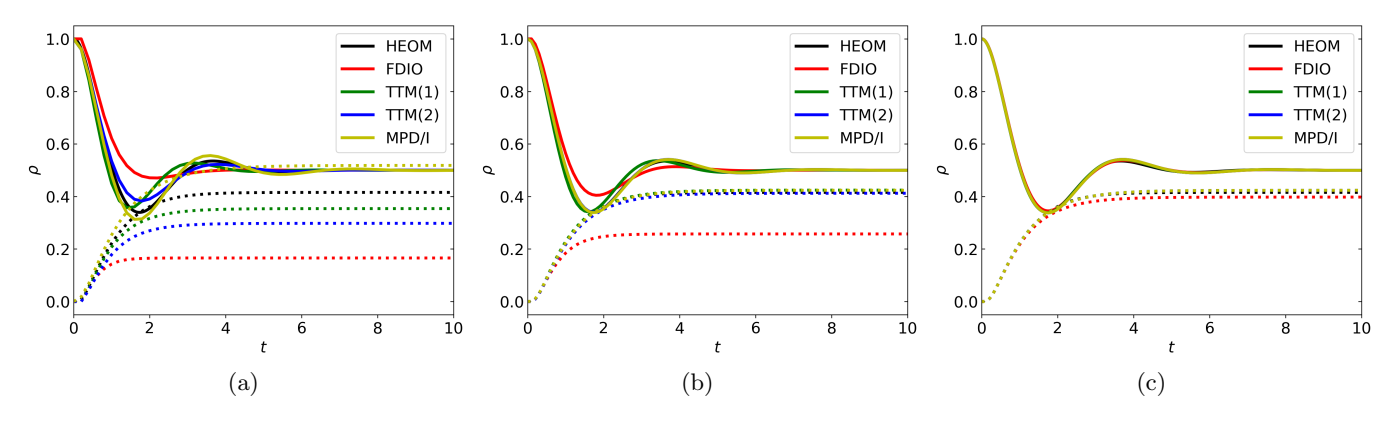


FIG. 3: RDM elements  $\text{Re}\rho_{00}$  (solid) and  $\text{Re}\rho_{01}$  (dotted) as a function of time. In each panel, black curves are computed from HEOM with  $\Delta t = 0.0005$ . FDIO, TTM(1), TTM(2), and MPI/D are plotted in corresponding colors with (a)  $\Delta t = 0.2$ , (b)  $\Delta t = 0.1$ , and (c)  $\Delta t = 0.01$ .

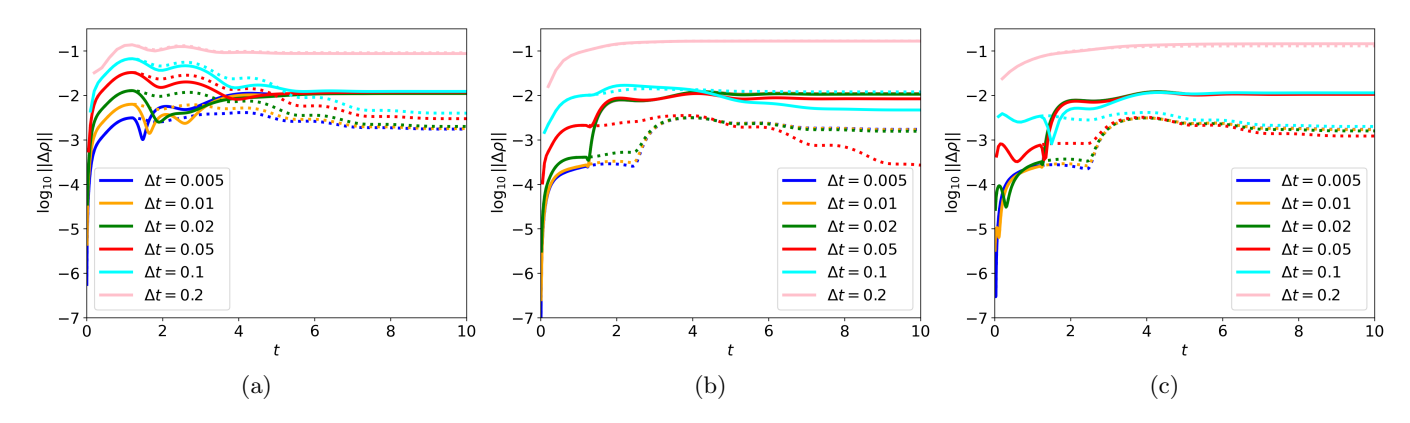


FIG. 4:  $\log_{10}(||\rho - \rho_{\text{HEOM}}||)$  as a function of time computed from (a) TTM(1), (b) TTM(2), (c) MPD/I. In each panel, solid and dotted curves are computed with memory cutoffs,  $t_{\text{mem}} = 1.2$  and 2.4, respectively. Different time step sizes  $\Delta t$  are plotted in corresponding colors.

time points, offering a resolution to the issues discussed in Ref. 28. The relationship was verified via numerical simulations using the spin-boson model. We observed that the elements of  $\mathcal{K}_N$  computed from discrete-time exact dynamical channels,  $U_N$ , converge to the exact result as  $\Delta t \to 0$ . Furthermore,  $K_N$  computed from exact  $\mathcal{K}_N$  leads to accurate discrete-time dynamics for sufficiently small  $\Delta t$  ( $\Delta t \leq 0.1$ ).

As discussed in Ref. 28, the discretization of NZ-QME is not unique. Alternatives, such as the midpoint derivative/midpoint integral (MPD/I) scheme proposed in Ref. 28, may offer practical advantages. In the spin-boson model example, MPD/I is found to be more efficient in generating accurate short time dynamics from exact  $\mathcal{K}_N$ , while the TTM discretizations provide  $\mathcal{K}_N$  from discrete-time exact dynamical channels with better convergence properties as  $\Delta t \to 0$ .

#### DATA AVAILABILITY

Data generated in this study is available on GitHub (https://github.com/JoonhoLee-Group/GQME\_discretization\_error.git).

### CODE AVAILABILITY

Simulation codes used in this study are available on GitHub (https://github.com/JoonhoLee-Group/GQME\_discretization\_error.git).

### ACKNOWLEDGEMENTS

R.P. and J.L. were supported by the U.S. Department of Energy, Office of Science, Accelerated Research in Quantum Computing Centers, Quantum Utility through Advanced Computational Quantum Algorithms, grant no. DE-SC0025572. L.P.L. acknowledges the support of

- S. Nakajima, On quantum theory of transport phenomena: Steady diffusion, Progress of Theoretical Physics 20, 948 (1958).
- [2] R. Zwanzig, Ensemble method in the theory of irreversibility, The Journal of Chemical Physics 33, 1338 (1960).
- [3] F. Ivander, L. P. Lindoy, and J. Lee, Unified framework for open quantum dynamics with memory, Nature Communications 15, 8087 (2024).
- [4] R. Feynman and F. Vernon, The theory of a general quantum system interacting with a linear dissipative system, Annals of Physics 24, 118 (1963).
- [5] N. Makri and D. E. Makarov, Tensor propagator for iterative quantum time evolution of reduced density matrices. i. theory, The Journal of Chemical Physics 102, 4600 (1995).
- [6] D. E. Makarov and N. Makri, Path integrals for dissipative systems by tensor multiplication. condensed phase quantum dynamics for arbitrarily long time, Chemical Physics Letters 221, 482 (1994).
- [7] N. Makri, Small matrix path integral with extended memory, Journal of Chemical Theory and Computation 17, 1 (2021), pMID: 33430598.
- [8] N. Makri, Small matrix disentanglement of the path integral: Overcoming the exponential tensor scaling with memory length, The Journal of Chemical Physics 152, 041104 (2020).
- [9] M. Kilgour, B. K. Agarwalla, and D. Segal, Path-integral methodology and simulations of quantum thermal transport: Full counting statistics approach, The Journal of Chemical Physics 150, 084111 (2019).
- [10] L. Simine and D. Segal, Path-integral simulations with fermionic and bosonic reservoirs: Transport and dissipation in molecular electronic junctions, The Journal of Chemical Physics 138, 214111 (2013).
- [11] N. Makri, Modular path integral methodology for realtime quantum dynamics, The Journal of Chemical Physics 149, 214108 (2018).
- [12] S. Kundu and N. Makri, Pathsum: A c++ and fortran suite of fully quantum mechanical real-time path integral methods for (multi-)system + bath dynamics, The Journal of Chemical Physics 158, 224801 (2023).
- [13] F. Bloch, Nuclear induction, Phys. Rev. **70**, 460 (1946).
- [14] A. G. Redfield, On the theory of relaxation processes, IBM Journal of Research and Development 1, 19 (1957).
- [15] E. Mulvihill and E. Geva, A road map to various pathways for calculating the memory kernel of the generalized quantum master equation, The Journal of Physical Chemistry B 125, 9834 (2021), pMID: 34424700.
- [16] M.-L. Zhang, B. J. Ka, and E. Geva, Nonequilibrium quantum dynamics in the condensed phase via the generalized quantum master equation, The Journal of Chemical Physics 125, 044106 (2006).
- [17] Q. Shi and E. Geva, A new approach to calculating the memory kernel of the generalized quantum master equation for an arbitrary system—bath coupling, The Journal of Chemical Physics 119, 12063 (2003).

- [18] E. Mulvihill, A. Schubert, X. Sun, B. D. Dunietz, and E. Geva, A modified approach for simulating electronically nonadiabatic dynamics via the generalized quantum master equation, The Journal of Chemical Physics 150, 034101 (2019).
- [19] L. Kidon, H. Wang, M. Thoss, and E. Rabani, On the memory kernel and the reduced system propagator, The Journal of Chemical Physics 149, 104105 (2018).
- [20] S. Chatterjee and N. Makri, Real-time path integral methods, quantum master equations, and classical vs quantum memory, The Journal of Physical Chemistry B 123, 10470 (2019), pMID: 31721584.
- [21] J. Cerrillo and J. Cao, Non-markovian dynamical maps: Numerical processing of open quantum trajectories, Phys. Rev. Lett. 112, 110401 (2014).
- [22] F. A. Pollock, E. Gull, K. Modi, and G. Cohen, Reduced Dynamics of Full Counting Statistics, SciPost Phys. 13, 027 (2022).
- [23] A. A. Kananenka, C.-Y. Hsieh, J. Cao, and E. Geva, Accurate long-time mixed quantum-classical liouville dynamics via the transfer tensor method, The Journal of Physical Chemistry Letters 7, 4809 (2016), pMID: 27934045.
- [24] M. Buser, J. Cerrillo, G. Schaller, and J. Cao, Initial system-environment correlations via the transfer-tensor method, Phys. Rev. A 96, 062122 (2017).
- [25] A. Gelzinis, E. Rybakovas, and L. Valkunas, Applicability of transfer tensor method for open quantum system dynamics, The Journal of Chemical Physics 147, 234108 (2017).
- [26] F. A. Pollock and K. Modi, Tomographically reconstructed master equations for any open quantum dynamics, Quantum 2, 76 (2018).
- [27] M. R. Jørgensen and F. A. Pollock, Discrete memory kernel for multitime correlations in non-markovian quantum processes, Phys. Rev. A 102, 052206 (2020).
- [28] N. Makri, Discrete generalized quantum master equations, Journal of Chemical Theory and Computation 0, null (0), pMID: 40326041.
- [29] W. H. Young, On the multiplication of successions of fourier constants, Proceedings of the Royal Society of London. Series A, Containing Papers of a Mathematical and Physical Character 87, 331 (1912).
- [30] V. I. Bogachev, Measure Theory, 2007th ed., Vol. 1 (Springer, Berlin, Germany, 2006).
- [31] A. Kelly, A. Montoya-Castillo, L. Wang, and T. E. Markland, Generalized quantum master equations in and out of equilibrium: When can one win?, The Journal of Chemical Physics 144, 184105 (2016).
- [32] E. Mulvihill and E. Geva, Simulating the dynamics of electronic observables via reduced-dimensionality generalized quantum master equations, The Journal of Chemical Physics 156, 044119 (2022).
- [33] A. Montoya-Castillo and D. R. Reichman, Approximate but accurate quantum dynamics from the mori formalism: I. nonequilibrium dynamics, The Journal of Chemical Physics 144, 184104 (2016).

- [34] A. Montoya-Castillo and D. R. Reichman, Approximate but accurate quantum dynamics from the mori formalism. ii. equilibrium time correlation functions, The Journal of Chemical Physics 146, 084110 (2017).
- [35] D. Brian and X. Sun, Generalized quantum master equation: A tutorial review and recent advances, Chinese Journal of Chemical Physics 34, 497 (2021).
- [36] Note that in Table 1 of Ref. 28 there is an additional factor of 1/2 from T to  $\mathcal{K}$ , which we believe is a typo from comparing their Eq. (33) and (36), and this was also numerically confirmed.
- [37] Y. Tanimura and R. Kubo, Time evolution of a quantum system in contact with a nearly gaussian-markoffian noise bath, Journal of the Physical Society of Japan 58, 101 (1989).
- [38] Y. Tanimura, Numerically "exact" approach to open quantum dynamics: The hierarchical equations of motion (heom), The Journal of Chemical Physics 153, 020901 (2020).
- [39] M. Xu, Y. Yan, Q. Shi, J. Ankerhold, and J. T. Stockburger, Taming quantum noise for efficient low temperature simulations of open quantum systems, Phys. Rev. Lett. 129, 230601 (2022).

- [40] Q. Shi, Y. Xu, Y. Yan, and M. Xu, Efficient propagation of the hierarchical equations of motion using the matrix product state method, The Journal of Chemical Physics 148, 174102 (2018).
- [41] E. Mangaud, A. Jaouadi, A. Chin, and M. Desouter-Lecomte, Survey of the hierarchical equations of motion in tensor-train format for non-markovian quantum dynamics, The European Physical Journal Special Topics 232, 1847 (2023).
- [42] Y. Yan, M. Xu, T. Li, and Q. Shi, Efficient propagation of the hierarchical equations of motion using the tucker and hierarchical tucker tensors, The Journal of Chemical Physics 154, 194104 (2021).
- [43] E. Mangaud, A. Jaouadi, A. Chin, and M. Desouter-Lecomte, Survey of the hierarchical equations of motion in tensor-train format for non-markovian quantum dynamics, The European Physical Journal Special Topics 232, 1847 (2023).
- [44] L. P. Lindoy, D. Rodrigo-Albert, Y. Rath, and I. Rungger, pyttn: An open source toolbox for open and closed system quantum dynamics simulations using tree tensor networks (2025), arXiv:2503.15460 [quant-ph].
- [45] Y. Nakatsukasa, O. Sète, and L. N. Trefethen, The aaa algorithm for rational approximation, SIAM Journal on Scientific Computing 40, A1494 (2018).